METAL NANOPARTICLE FABRICATION WITH MULTIPLE CAPPING LIGANDS VIA A MICROFLUIDIC DEVICE

Cade Christensen,* Porter Wilkes,* Chase Garrett,* Taytum Stratton,* Jonah Babbel,* Payton Riggs,* Sacha Toussaint,* Brittany Christensen,* Payden Harrah,* Kyler Radmall,* Rachel Radmall,* Nakelle Goldie,* Simon Langlois,* Seth Wetjen,* Samuel Hodnett,* Max Brown,* Christopher F. Monson†

Physical Science Department, Southern Utah University, Cedar City, UT 84720

Abstract

A microfluidic device was developed to fabricate silver, gold, and manganese nanoparticles. Nanoparticle formation was verified through fluorescence characterization of the resulting nanoparticle solutions and SEM imaging of the nanoparticles. Silver nanoparticle formation was the most extensively investigated, and many sets of conditions resulted in nanoparticle solutions of sufficient concentration that the emission peak was significantly red-shifted (to ~550 or ~600 nm) compared to the peak observed in diluted solutions (~455 or ~465 nm). Biologically relevant molecules (proteins and to a lesser extent lipids) were shown to act as ligands forming reproducible silver nanoparticles. When gold nanoparticles were formed, it was shown that the size of the nanoparticles could be increased by increasing the reaction time before capping ligands were added. Manganese nanoparticles were formed using a similar procedure in the same microfluidic device used for the silver and gold nanoparticles, and were most likely manganese phosphate and/or manganese hydroxide.

†Corresponding author: christophermonson1@suu.edu *Undergraduate researchers and co-authors
Keywords: Silver, gold, and manganese nanoparticles, biological ligands, microfluidic device
Received: January 7, 2025 Accepted: January 28, 2025 Published: February 4, 2025

Introduction

Nanoparticles and nanomaterials in general have proven to be both versatile and useful in applications as diverse as antibacterials,[1] electronics fabrication,[2] and many other areas.[3,4] One of the characteristics of nanoparticles that results in their high utility is that their properties are, in large part, determined by their size and shape.[5,6] Accordingly, many methods have been developed to control the size and shape of nanoparticles: most commonly by varying the capping ligand, but also using light,[7] solution characteristics during laser ablation,[8] and temperature-dependent precipitation of capping ligands[9] to name a few when making solution-phase nanoparticles. One of the common uses for nanoparticles is in sensors in which they commonly translate molecular events into macroscopic signals, for example in bacterial detectors.[10,11]

Nanoparticle interactions with both capping ligands and other materials can significantly alter both the nanoparticles and the ligand or other material properties.[5,12-14] Many different compounds will interact with nanoparticles, altering nanoparticle properties, for example spectroscopy including absorption and emission lines.[15,16] This is of particular interest with proteins, as proteins are biologically important and known to interact with nanoparticles.[5]

Nanoparticle fabrication is often performed via a single-pot method, in which all reagents are combined in a single reaction vessel, but fabrication using microfluidic devices is also becoming common.[4,17-20] Microfluidic devices potentially offer additional control of the fabrication process compared to single-pot methods, as reaction times, conditions, and mixing can be more precisely controlled, thus having the potential to generate more uniform nanoparticles.[18] Microfluidic devices can be fabricated of many different materials, most commonly glass, plastic, or an elastomer like polydimethyl siloxane (PDMS). Many methods for fabricating microfluidic devices have been reported, including photolithographic methods, masters or molds, and sacrificial methods.[21-24] We report the synthesis of a microfluidic device using a simple and inexpensive sacrificial method not previously employed for nanoparticle fabrication and its use in the fabrication of nanoparticles of three different metals (Ag, Au, and Mn) and with several ligands, including small molecules, a lipid, and proteins. The nanoparticles formed were anlayzed to determine both their spectroscopic and size characteristics..

Experimental Methods

Device Fabrication

Devices were fabricated via a sacrificial method, using a magnesium ribbon (Ginsberg Scientific, 4 mm x 0.2 mm) in PDMS (Sylgard 184, Dow). This method was previously used to fabricate microfluidic devices involved in reaction characterization.[25] Briefly, a magnesium ribbon was cut and bent to form the desired channel intersections and shapes and then suspended in liquid PDMS and the PDMS was baked to cure and solidify it. The PDMS/magnesium block was then sonicated in 2 M HCl (diluted from concentrated HCl, Fisher, ACS grade) until the magnesium ribbon was completely dissolved (up to several weeks) and the device was ready for use.

Nanoparticle Fabrication

Nanoparticles were fabricated in the microfluidic device using aqueous solutions of all reagents. In all cases, the metal ion and the reducing agent were put in the first two inlets on the device (see Figure 1 for a device illustration). In all cases, solution introduction was controlled with syringe pumps (New Era 300 syringe pump, new Era Pump Systems Inc.). Sodium hydroxide was put into the third inlet on the device and the solutions were then mixed by a twist in the channel (the metal ion and reducing agent previously were flowing next to each other without mixing to create nucleation sites at their solution junction). The channel twisted over several cm of the device to thoroughly mix the

solutions and allow nanoparticle growth to proceed. The capping ligand was added at the fourth inlet, the solution was once again mixed, and the finished nanoparticles exited the device and were collected in vials, typically in aliquots of a few mL. Solution composition and concentrations are detailed in Table 1. Every 3-5 runs the device was cleaned by placing it in a sonicator with 2 M HCl for at least 15 minutes or by running 6 M nitric acid through the device.

Nanoparticle characterization

Nanoparticles were characterized by UV-Vis, fluorescence spectroscopy, and SEM. The solutions were allowed to sit for at least one hour before being analyzed, as it was noted that changes in the appearance and spectra of the solutions sometimes occurred after the solution was made. Unless degradation was being studied, the solutions were analyzed within two days of being made. However, many nanoparticle solutions were observed to be stable over extended periods of time (up to several years). When analyzing fluorescence, the nanoparticles were generally excited using 350 nm light, although a range of different wavelengths were initially explored.

Results and Discussion

Microfluidic device

A representation of the microfluidic device used is shown in Figure 1. Device fabrication using this method is both simple and inexpensive, requiring only a vacuum system to degas the PDMS and a sonicator to dissolve the magnesium ribbon. Due to the low materials and equipment costs, this microfluidic fabrication method could be applicable in many circumstances where traditional microfluidics are not practical due to cost or microfluidic fabrication equipment limitations, such as in undergraduate laboratories. It should be noted that each device was hand made and thus the exact device dimensions varied slightly. However, the general device dimensions are: the channel was 200 µm tall and around 1.5 mm wide, with a total length of around 12 cm. The microfluidic device itself was approximately 1 cm wide, 1 cm tall, and 6-10 cm long (the variation was largely due to the amount of bending in the channel, which varied with each device).

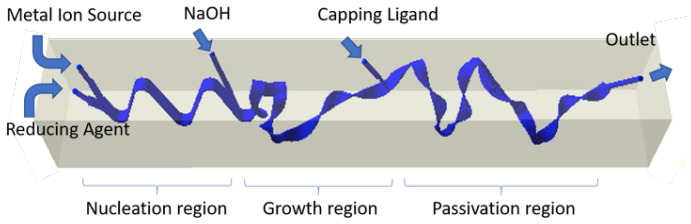

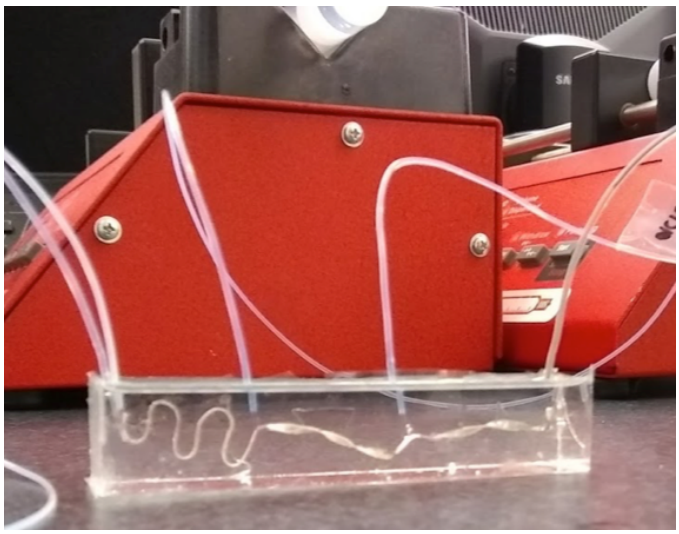

Figure 1. Top: An illustration of the microfluidic device. It has four inlets, one outlet, and three distinct regions. From left to right, metal ions and reducing agents are introduced into the first two inlets. The solutions travel next to each other without significant mixing taking place to allow nanoparticle nucleation at the fluid junction. In the third inlet, NaOH is typically added and the solutions are mixed to allow nanoparticle growth. The capping ligand is added in inlet four and the solutions are once again mixed, before being collected at the outlet. Bottom: a photo of an actual device with syringe pumps in the background.

The first third of the channel length consisted of a nucleation region in which the channel undulates vertically in the device but does not twist. In this region, laminar flow predominates, and the two solutions do not mix except where the two solutions touch. This is designed to allow nanoparticle nucleation to occur. The nucleation region ends when sodium hydroxide solution is added and the channel twists. The twist in the channel mixes the solutions, as has been shown previously.[25] Additionally, herringbone patterns were added to the magnesium wire by scratching it with a razor blade in regions with twists, which assist in mixing. The solution mixing and alkalinization allows the nucleation sites generated in the first third of the device to grow over the middle third of the device.

The final third of the device begins with the capping ligand being added and then the solutions are again mixed with twists and herringbone patterns for the balance of the device channel. In this region of the device, the nanoparticles are passivated with the capping ligand to halt nanoparticle growth, although additional growth on unpassivated faces of the nanoparticle is possible.

Table 1: Solutions used in nanoparticle fabrication.

Inlet	Reagent	Concentrations
Silver Nanoparticles		
Metal ion source (first inlet):	Silver nitrate (Alfa Aesar, 99.9+%)	3, 4, 6.5, 10, 12, 20 mM
Reducing agent (second inlet):	Ascorbic acid (Fisher, reagent grade)	5, 10, 20 mM
Third inlet:	Sodium hydroxide (Fisher, reagent grade)	10, 15, 20, 30, 60 mM
Capping ligands (fourth inlet):	Citric acid (Fisher)	5, 10, 20 mM
	DOPS (lipid, Avanti polar lipids)	1 mg/mL
	BSA (protein, Sigma Aldrich)	0.2, 0.57, 1.3, 2, 15 mg/mL
	Casein (protein Alfa Aesar)	0.35, 0.39, 1.3, 2, 12 mg/mL
	Riboflavin (Vitamin B2, AppliChem)	Saturated (<1 mM)
Gold Nanoparticles		
Metal ion source (first inlet)	Tetrachloroauric (III) acid (Alfa Aesar, 99.99%)	3 mM
Reducing agent (second inlet)	Ascorbic acid	10 mM
Third inlet	Sodium hydroxide	20 mM
Capping ligands (fourth inlet)	Citric acid	10 mM
Manganese Nanoparticles		
Metal ion source (first inlet)	Manganese (II) acetate (Matheson Coleman)	10 mM
Reducing agent (second inlet)	Sodium dithionite (J.T. Baker)	15 mM
Third inlet	Nothing (capped)	
Capping ligands (fourth inlet)	Oleic acid (Fisher, lab grade) and NaOH	20 mM oleic acid in 0.1 M NaOH
	BSA (protein, Sigma Aldrich)	0.2, 1.0 mg/mL
	Casein (protein Alfa Aesar)	0.2, 1.0 mg/mL
	FusionRed (protein, expressed in-house, in phosphate buffer)	0.2 mg/mL

Thus, the nanoparticles should be finished upon exiting the device. While some small changes in nanoparticle solutions were observed over the first hour after exiting the device, these changes were usually silver metal precipitation when smaller quantities of capping ligands or large quantities of silver ions were used, thus the nanoparticles were typically finished upon exiting the device as intended.

Silver Nanoparticle Solutions

Nanoparticle solutions produced using the microfluidics described above were characterized using UV-Vis and fluorescence. Fluorescence was typically found to be more informative, except with the gold nanoparticlesas UV-Vis has been previously shown to be both well characterized and high informative for gold nanoparitcles.The majority of the solutions produced by the microfluidic device were so concentrated that little fluorescence was observed until the solution was diluted, as can be seen in Figure 2. Thus, all solutions were diluted by a 1:50 ratio for analysis (50 µL of nanoparticle solution in 2 mL of deionized water) unless otherwise noted.

The observed shift in fluorescence wavelength emission maximum with dilution (as shown in Figure 2 left panel) is attributed to the dilution increasing the average spacing between nanoparticles. This has two primary effects. First, nanoparticle solutions were often made at such a high concentration that most nanoparticles were near enough to additional nanoparticles that they behaved like larger nanoparticles. On dilution, the average space between nanoparticles increased, and thus the fluorescence peak was blue-shifted. Second, nanoparticle absorbance was stronger in the blue region than in the red region, and thus at higher concentrations there was more secondary absorption of fluorescent photons and less light observed.[26,27]

Additionally, it was observed for a significant number of nanoparticle solutions that a silver metal solid collected on the bottom of the vial over time. These solutions usually retained the greenish-brown color that was indicative of nanoparticles but in a few solutions silver metal precipitation was severe enough that the solution went almost clear. This was principally due to larger nanoparticles and nanoparticle clusters growing to become silver microparticles, as can be seen by the significant reduction in fluorescence at the red end of the fluorescence spectra in the right-hand graph of Figure 2.

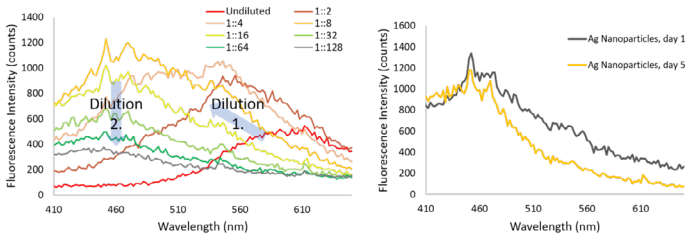

Figure 2. Silver nanoparticle solutions before and after dilution (left) and over time (right, diluted). As indicated by the arrows in the left panel, on dilution high concentration silver nanoparticle solution first shows a fluorescence emission blue shift with increasing intensity and then reaches a dilution at which the peaks are relatively stable. Further dilution decreases signal intensity but peak positions remain approximately unchanged. At right, the degradation of poorly passivated silver nanoparticles over four days is shown.

Flow and Concentration Rate Variation

One of the major advantages of using a microfluidic device relative to a one-pot synthesis is that changing the reagent ratio is simply a matter of changing the flow rates on the pumps. Thus, one of the first things investigated was the effect of changing the flow rates on the nanoparticle properties. Flow rates were varied from 0.010 to 0.40 mL/min of all reagents (silver nitrate, ascorbic acid, sodium hydroxide, and citric acid). Interestingly, this did not result in observable changes to nanoparticle solutions except for when sodium hydroxide flow rates were changed (See Figure 3). As illustrated in Figure 3 A, at low sodium hydroxide flow rates relatively large numbers of nanoparticles were formed, as can be seen by the red-shifted multiple nanoparticle peaks. As sodium hydroxide flow rates were increased nanoparticle concentrations first increased (at 0.15 mL/min the large red-shifted peak), then decreased, and then slightly increased (Figure 3A)

An interesting feature of both the flow rate and concentration variation data is that, at least when nanoparticles are sufficiently dilute, at least two and often four peaks commonly appear: a peak at around 450 nm and a second around 465 nm (highlighted by vertical dashed lines in Figure 3 A), as well as peaks at 550 nm and 615 nm (visible as shoulders or peaks in Figure 3 A). In addition to these relatively narrow peaks (see Figure 4 for them as well), broad peaks in the red-shifted regions can appear that we attribute to nanoparticle aggregation (as shown in Figure 2). However, as

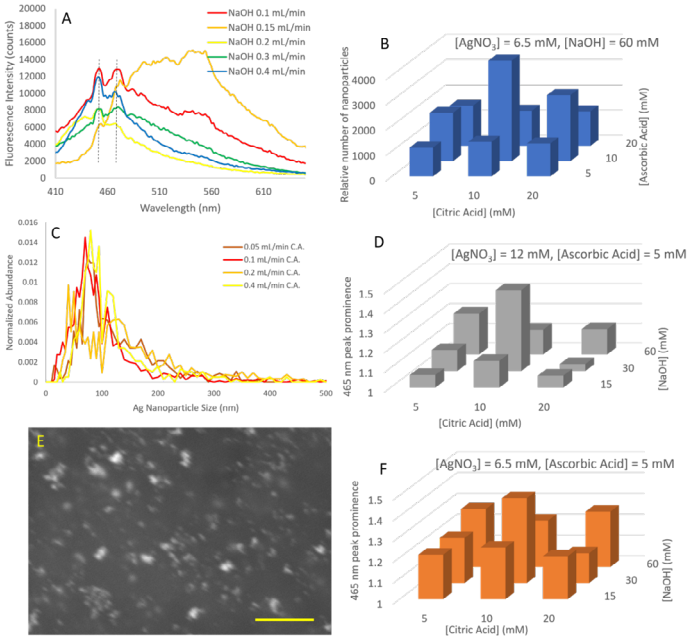

Figure 3. The effects of changing flow rates and concentration on silver nanoparticle formation. Panel A illustrates how silver nanoparticle solutions change when the sodium hydroxide flow rate is changed (other conditions: silver nitrate 4 mM, 0.03 mL/min, ascorbic acid 10 mM, 0.15 mL/min, citric acid 10 mM, 0.1 mL/min, sodium hydroxide 20 mM). For this graph solutions were not diluted as the silver concentration was relatively low. Panels B, D, and F illustrate the observed variations when nanoparticles were formed with different concentrations of reagents. B: the approximate variation in the total number of nanoparticles formed when citric acid and ascorbic acid were varied. D and F: the prominence of the 465 nm peak when citric acid and sodium hydroxide are varied at two different silver nitrate concentrations (12 mM and 6.5 mM). Panels C and E illustrate changes in flow rate of citric acid (binding ligand) as measured by SEM. In both panels, silver nitrate 6 mM 0.1 mL/min, ascorbic acid 10 mM 0.1 mL/min, NaOH 20 mM 0.1 mL/min, citric acid 10 mM. C: histogram of particle sizes. E: representative SEM image at 0.05 mL/min citric acid, scale bar is 1 µm.

can be seen in the 0.2 mL/min run in the left panel of Figure 3 A, at times an additional peak appears at around 430 nm. Solutions that exhibit this peak tend to have unstable nanoparticles, and due to both the blue-shifted nature and instability observed, we attribute this peak to smaller, poorly passivated (poorly covered with capping ligand) nanoparticles that react with the better-passivated nanoparticles and cause them to grow to microparticles and precipitate.

The concentrations of the four reagents (silver nitrate, ascorbic acid, sodium hydroxide, and citric acid) were varied systematically, with each tested at a lower, mid, and high concentration (5, 10, 20 mM for citric and ascorbic acid, 10, 30, 60 mM for NaOH and 6.5, 12, 20 mM for silver nitrate). While most effects observed were relatively small, when silver concentrations were changed from 6.5 mM to 12 mM to 20 mM, the nanoparticle solutions went from stable to highly unstable, falling out of solution as silver microaggregates in days. Thus, no data is shown for 20 mM silver concentrations, as the nanoparticle solutions never exhibited sufficient stability. Additionally, some 12 mM silver nitrate runs produced nanoparticles that were too unstable to reliably characterize, so these data are not shown.

The relative concentrations of nanoparticles synthesized is shown in two different ways in Figure 3 (Figure 3 panels B, D, and F). First, panel B shows an estimate of the number of nanoparticles formed, obtained from the diluted nanoparticle solutions. This estimate was obtained by multiplying the observed fluorescent counts around 600 nm by 3, multiplying the counts around 550 nm by 2 and adding those two quantities to the average observed fluorescent counts around 450 nm. This roughly serves to account for nanoparticle aggregation, although it is likely still

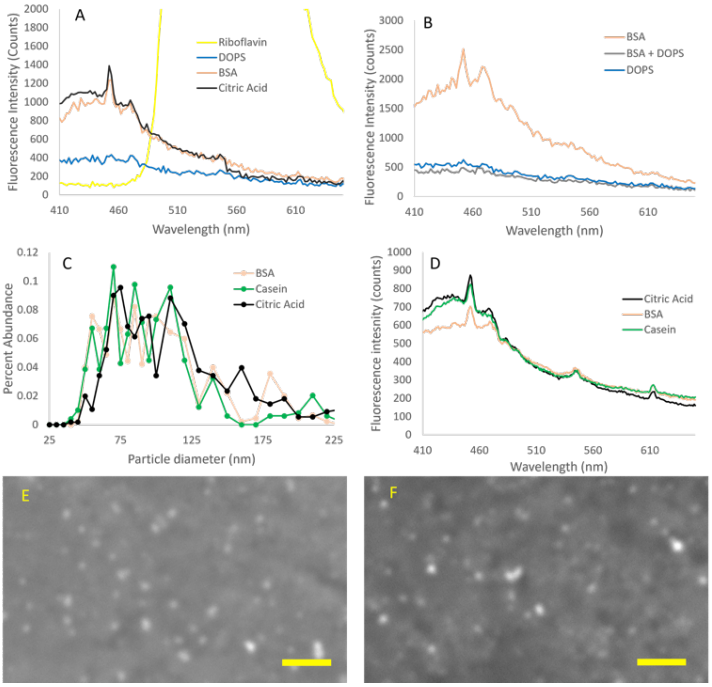

Figure 4. Silver nanoparticles with biologically relevant ligands. Panel A shows the fluorescence signals obtained when riboflavin, DOPS, BSA, and citric acid were used as ligands. Panel B shows a comparison of BSA, DOPS, and a mixture of the two. Panels C and D show a comparison of BSA, Casein (two proteins), and citric acid (a small molecule ligand) using SEM data (Panel C) and fluorescence (Panel D). Panels E and F show representative images obtained with BSA (E) and Casein (F) as ligands. Scale bars are 500 nm.

an underestimate for aggregated nanoparticles as it does not account for secondary absorbance. As can be seen in the graph, the greatest number of nanoparticles forms when 10 mM citric acid and 10 mM ascorbic acid are used with 6.5 mM silver nitrate and 60 mM sodium hydroxide. This observation led to the use of these concentrations of sodium hydroxide and ascorbic acid as the "standard conditions" for our work with biologically-relevant ligands (below, Figure 4).

The second method of determining relative concentrations of nanoparticles in solution focused on the prominence of various peaks (Figure 3 panels D and F). Due to its variability and relatively large size of the peak, both of the graphs shown focus on the 465 nm peak. As can be seen in the Figure 3 A and in Figure 4, the peak at 465 nm varies from large and well-defined to a shoulder. The prominence of this peak was calculated by dividing the observed fluorescent counts at the 465 nm peak by the fluorescent counts at 480 nm, which was beyond the edge of the peak by a small amount but just at the edge of the shoulder. Thus a number greater than one implies a peak and the larger the number, the more prominent the peak. On the other hand, a number less than or equal to one implies no peak. As can be seen in Figure 3, in this case 10 mM citric acid and 30 mM sodium hydroxide resulted in the best defined peaks (at 5 mM ascorbic acid and both 6.5 and 12 mM silver nitrate concentrations). It should be noted that a method of calculating the 465 nm peak prominence was also examined using an average of the 480 nm fluorescence counts (to the right of the 465 nm peak) and the counts to the left of the peak at 436 nm. This produced broadly similar results that were less pronounced.

Biological Ligands with Silver Nanoparticles

One of the attractive features of silver nanoparticle fabrication with microfluidics is the ability to test ligands that are relatively weakly binding. This is because when biological ligands are added to nanoparticles as they are grown in a microfluidic device, the ligands do not need to displace any existing capping ligands to bind to the nanoparticles. On the other hand, when nanoparticles are first grown (in a one-pot synthesis or a microfluidic device) and then exposed to biological molecules, the binding of the biological molecules to the nanoparticles depends on the ability of the biological molecules to either bind to the nanoparticle-capping ligand combination or displace the capping ligand. Thus, we were hopeful that using biological ligands would result in new and distinguishable nanoparticles being formed.

As can be seen in Figure 4, multiple potential biological ligands of several different molecular classes were tested. A small molecule (riboflavin), a lipid (DOPS), and two proteins (BSA and casein) were tested as ligands as well as the previously used ligand citric acid. In the case of riboflavin, any nanoparticles that may have formed had their fluorescence emission absorbed by the riboflavin itself, although it should be noted that a significant amount of silver debris was observed in that bottom of the vial and thus it is thought that few or no stable nanoparticles were formed. Using DOPS as a ligand also resulted in a significant amount of silver debris in the vial, although a weak fluorescence signal was observed, denoting some silver nanoparticles were formed. The two peaks typically observed (at 445 and 465 nm) were barely or not at all present with both these ligands.

When proteins were tested as ligands, the nanoparticles formed are much more similar fluorescently to those formed using citric acid, with similar peaks at 445, 465, 545 and 615 nm (Figure 4). Two proteins were tested as ligands – BSA and casein – and both resulted in the formation of "typical" nanoparticles with peaks at 445 and 465 nm. However, as can be seen in Figure 4 D, the nanoparticles made with casein as the ligand showed a much less pronounced peak at 465 nm. SEM analysis showed that nanoparticles made using citric acid, BSA, and casein all had similar size distributions (Figure 4 C). We also examined the effect of varying the concentration and flow rates of the biological ligands on the nanoparticles formed. We found no significant reproducible difference between the concentrations tested.

Additionally, mixtures of ligands were tested. These are of interest because biological molecules typically occur in a complex milieu of molecules and the direct use of biological fluids as a ligand source (in disease diagnosis applications, for example) would be highly convenient. As can be seen in Figure 4 B, DOPS and BSA behave very differently with respect to nanoparticle formation – DOPS forms relatively few nanoparticles while BSA forms large numbers of nanoparticles. When BSA and DOPS are mixed, the solution behaves almost identically to pure DOPS. We found this highly counterintuitive – based on the apparently favorable nanoparticle formation with BSA vs the unfavorable nanoparticle formation with DOPS, we thought that BSA-dependent nanoparticle formation should dominate. Perhaps the affinity of DOPS and phosphatidylserine lipids in general for positive ions results in the sequestration of free silver ions and the dissolution of nanoparticles,[28] or lipid-BSA interactions eliminated BSA-nanoparticle binding sites.[29,30]

Gold and Manganese Nanoparticles

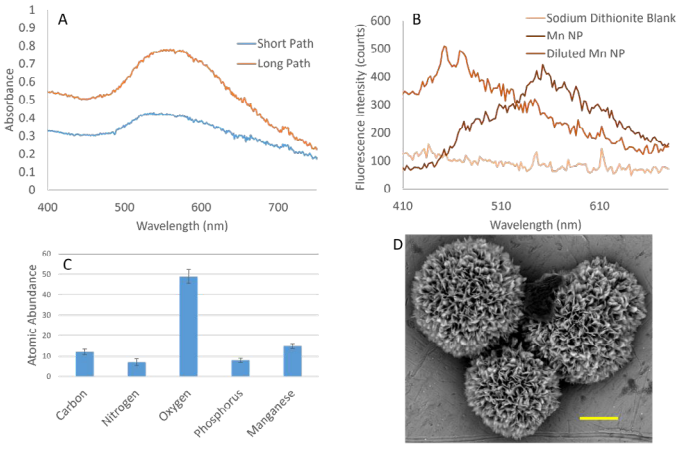

Figure 5. Gold and manganese nanoparticle formation using microfluidic devices. Panel A shows the absorbance of gold nanoparticles fabricated using a microfluidic device with a standard length nanoparticle growth section vs the same conditions but with a growth section approximately ten times longer. As can be seen, nanoparticles given more time to grow result in larger average sizes (more red-shifted absorbances). Panel B shows the fluorescence obtained when oleic-acid passivated manganese nanoparticles were formed, at the original concentration, when diluted, and compared to a sodium dithionite blank. Panel C shows the composition of the FusionRed passivated Mn nanoparticles as determined by EDS. Panel D shows a representative image of the FusionRed passivated Mn nanoparticles. Scale bar is 20 μm.

We also tested the ability of our microfluidic devices to form nanoparticles of materials other than silver. Gold nanoparticles are well studied and several microfluidic fabrication methods have previously been used,[19] so gold nanoparticle fabrication seemed like a logical extension of our initial work with silver. As can be seen in Figure 5 A, our devices were able to make gold nanoparticles. As mathematical relationships between nanoparticle absorbance and nanoparticle size are known[6,31] this also allowed us to calculate an average nanoparticle size. When a relatively short path microfluidic was used, (11 cm between mixing and capping ligand addition) the maximum absorbance was observed around 534 nm, which correlates to an average nanoparticle size of approximately 60 nm. When the long path was used, (the equivalent of 100 cm, although part of the length increase was achieved by widening the channel and thus decreasing the flow rate and increasing the residence time) the absorbance maximum was at 562 nm which gives an average size of 90 nm. Thus, as expected, a longer nanoparticle development time leads to larger nanoparticles.

In addition to gold nanoparticles, manganese was used to form nanoparticles. For these nanoparticles, manganese (II) acetate solution was mixed with sodium dithionite solution ($Na_2S_2O_4$). This resulted in a solution with a deep yellow or brown color that exhibited fluorescence, as shown in Figure 5 B. Additionally, when the solution was diluted, the peak shifted from around 550 nm to two peaks at 445 nm and 465 nm and increased slightly in intensity. Several different ligands were used, including proteins, but the most consistent and intricate nanoparticles were obtained using FusionRed protein, a green fluorescent protein (GFP)-related fluorescent protein.[32] Mn nanoparticles made with FusionRed were observed by SEM to have a "desert rose" shape (Figure 5 D), as we reported[33] and as has been reported for other transition metal complexes previously.[34] When we analyzed these nanoparticles with energy dispersive spectroscopy (EDS) to identify the elements present (Figure 5 C), the consistent presence of phosphorus and oxygen at relatively high levels leads us to believe the nanoparticles are made of manganese phosphate or a phosphate/hydroxide mix. This is consistent with other desert rose nanoparticles previously observed.[35,36] To our knowledge, this is the first published fabrication of manganese nanoparticles via a microfluidic device and one of a relatively few published methods to fabricate manganese nanoparticles.[37-40]

Conclusions

We have created microfluidic devices capable of fabricating metal nanoparticles using gold, silver and manganese metal ions with citric acid, DOPS, BSA, Casein, riboflavin, oleic acid, and FusionRed protein used as capping ligands. By changing the conditions and in particular the length of the channel over which the nanoparticles grow the nanoparticle growth can be controlled in predictable ways. Using different ligands also results in changes in the nanoparticles, although these changes are harder to predict. Nanoparticle creation was also observed when biologically relevant molecules were used as ligands, although so far only relatively minor differences between nanoparticles formed with traditional ligands such as citrate and those formed with protein ligands have been observed. Finally, manganese nanoparticles were successfully synthesized. These results suggest several possible future directions, including a means to facilitate a broader

use of customized nanoparticles in resource-limited laboratories and the investigation of manganese nanoparticles as catalysts due to their large surface area.

Acknowledgements

We thank John Terrel, Haley Philips, and Jaxson Jeffery for work they did related to this project. We thank the SUU faculty scholarly support fund, faculty project fund, and undergraduate research and scholarly program for funding. K.R. and R.R. thank the Walter Maxwell Gibson research fellowship for funding.

References

1. Valodkar, M.; Modi, S.; Pal, A.; Thakore, S. *Mat Res Bull* **2011**, *46*, 384–389.
2. Li, Y.; Wu, Y.; Ong, B. S.; *J Am Chem Soc* **2005**, *127*, 3266-3267.
3. Khaturia, S.; Chahar, M.; Sachdeva, H.; Sangeeta; Mahto, C. B. *J Nanomed Nanotech* **2020**, *11*, DOI 10.35248/2157-7439.20.11.543
4. Feng, Q.; Sun, J.; Jiang, X. *Nanoscale* **2016**, *8*, 12430-12443.
5. Boehmler, D. J.; O'Dell, Z. J.; Chung, C.; Riley, K. R. *Langmuir* **2020**, *36*, 1053-1061.
6. Haiss, W.; Thanh, N. T. K.; Aveyard, J.; Fernig, D. G. *Anal Chem* **2007**, *79*, 4215-4221.
7. Callegari, A.; Tonti, D.; Chergui, M. *Nano Lett* **2003**, *3*, 1565-1568.
8. Mafune, F.; Kohno, J.; Takeda, Y.; Kondow, T.; Sawabe, H.; *J Phys Chem B* **2000**, *104*, 9111-9117.
9. Morones, J. R.; Frey W. *Langmuir* **2007**, *23*, 8180-8186.
10. Wang, R.; Xu, Y.; Sors, T.; Irudayaraj J.; Ren W.; Wang R. *Microchim Acta* **2018**, *185*, 184.
11. Yang, P.; Ding, Z.; Li, X.; Dong, Y.; Fu, T.; Wu, Y. *Anal Chem* **2019**, *91*, 12134-12137.
12. Mariam, J.; Dongre, P. M.; Kothari, D. C. *J Fluoresc* **2011**, *21*, 2193.
13. Putra, R. P.; Ikumura, Y.; Horino, H.; Hori, A; Rzeznicka, I. I. *Langmuir* **2019**, *35*, 16576-16582.
14. Li, X.; Lenhart, J. J.; Walker, H.W. *Langmuir* **2012**, *28*, 1095-1104.
15. Fernando, I.; Zhou, Y. *Chemosphere* **2019**, *216*, 297-305.
16. Abdelhalim, M. A. K.; Mady, M. M.; Ghannam, M. M *J Nanomed Nanotech* **2012**, *3*, DOI 10.4172/2157-7439.1000133.
17. Hung, L. -H.; Lee, A. P. *J Med Biol Eng* **2007**, *27*, 1-6.
18. Liu, D.; Cito, S.; Zhang, Y.; Wang, C. -F.; Sikanen, T. M.; Santos, H. A. *Adv Mat* **2015**, *27*, 2298.
19. Ma, J.; Lee, S. M. -Y. ; Yi, C.; Li, C. -W. *Lab Chip* **2017**, *17*, 209-226.
20. Tang, S. -Y.; Qiao, R.; Yan, S.; Yuan, D.; Zhao, Q.; Yun, G.; Davis, T. P.; Li, W. *Small* **2018**, DOI 10.1002/smll.201800118.
21. Raj, K. M.; Chakraborty, S. *J App Polymer Sci* **2020**, DOI 10.1002/APP.48958
22. Elvira, K. S.; Casadevall i Solvas, X.; Wootton, R. C. R.; de-Mello, A. J. *Nature Chem* **2013**, *5*, 905-915.
23. Eves, D. J.; Woolley, A. T. *Anal Bioanal Chem* **2009**, *393*, 431-435.
24. Robison, A. D.; Finkelstein, I. J. *Anal Chem* **2014**, *86*, 4157-4163.
25. Barney, J.; Torgersen, T.; Monson, C. F. *J Utah Acad* **2018**, *95*, 235-249.
26. Pucci, A.; Boccia, M.; Galembeck, F.; Leite, C. A. P.; Tirelli, N.; Ruggeri, G. *Reactive Functional Polymers* **2008**, *68*, 1144-1151.
27. Sportelli, M. C.; Izzi, M.; Volpe, A.; Clemente, M.; Picca, R. A.; Ancona, A.; Lugara, P. M.; Palazzo, G.; Cioffi, N. *Antibiotics* **2018**, *7*, doi:10.3390/antibiotics/7030067.
28. Monson, C. F.; Cong, X.; Robison, A. D.; Pace, H. P.; Liu, C.; Poynton, M. F.; Cremer, P. S. *J Am Chem Soc* **2012**, *134*, 7773-7779.
29. Kundu, S.; Matsuoka, H.; Seto, H. *Coll Surf B: Biointerfaces* **2012**, *93*, 215-218.
30. Lystvet, S. M.; Volden, S.; Yasuda, M.; Halskau, O.; Glomm, W. R. *Nanoscale* **2011**, *3*, 1788-1797.
31. Martinez, J. C.; Chequer, N. A.; Gonzalez, J. L.; Cordova, T. *Nanosci Nanotech* **2012**, *2*, 184-189.
32. Shemiakina, I. I.; Ermakova, G. V.; Cranfill, P. J.; Baird, M. A.; Evans, R. A.; Souslova, E. A. et al. *Nat Comm* **2012**, *3*, 1204.
33. Stratton, T.; Pierce, E.; Monson, C. F. *J Utah Acad* **2022**, *99*, 261-273.
34. Dega, N. K.; Ganganboina, A. B; Tran, H. L.; Kuncoro, E. P.; Doong, R. *Talanta* **2022**, *237*, 122957.
35. Ge, J: Lei, J; Zare, R. *Nature Nanotech* **2012**, *7*, 428-432.
36. Pardhiya, S.; Priyadarshini, E.; Rajamani, P. *Appl Sci* **2020**, *2*, 1597.
37. Kamran, U.; Bhatti, H. N.; Iqbal, M.; Jamil, S.; Zahid, M. *J Molec Struc* **2019**, *1179*, 532-539.
38. Bondi, J. F.; Oyler, K. D.; Ke, X.; Schiffer, P.; Schaak, R. E. *J Am Chem Soc* **2009**, *131*, 9144-9145.
39. Jayandran, M.; Haneefa, M. M.; Balasubramanian, V. *J App Pharm Sci* **2015**, *5*, 105-110.
40. Zhen, Z.; Xie, J. *Theranostics* **2012**, *2*, 45-54.